Biochimica et Biophysica Acta 1838 (2014) 1832–1841

Contents lists available at ScienceDirect

Biochimica et Biophysica Acta

journal homepage: www.elsevier.com/locate/bbamem

Boundary region between coexisting lipid phases as initial binding sites for *Escherichia coli* alpha-hemolysin: A real-time study

Sabina M. Maté [a,*], Romina F. Vázquez [a], Vanesa S. Herlax [a], María A. Daza Millone [b], María L. Fanani [c], Bruno Maggio [c], María E. Vela [b], Laura S. Bakás [a,d]

[a] Instituto de Investigaciones Bioquímicas de La Plata (INIBIOLP), CCT—La Plata, CONICET, Facultad de Ciencias Médicas, Universidad Nacional de La Plata, 60 y 120, (1900) La Plata, Argentina
[b] Instituto de Investigaciones Fisicoquímicas Teóricas y Aplicadas (INIFTA), Universidad Nacional de La Plata—CONICET, Sucursal 4 Casilla de Correo 16, 1900 La Plata, Argentina
[c] Centro de Investigaciones en Química Biológica de Córdoba (CIQUIBIC), UNC—CONICET, Dpto. de Química Biológica, Fac. Cs. Químicas, UNC, Haya de la Torre y Medina Allende, Ciudad Universitaria, Córdoba, Argentina
[d] Departamento de Ciencias Biológicas, Facultad de Ciencias Exactas, Universidad Nacional de La Plata, 47 y 115, 1900 La Plata, Argentina

ARTICLE INFO

Article history:
Received 3 September 2013
Received in revised form 24 February 2014
Accepted 27 February 2014
Available online 7 March 2014

Keywords:
Pore-forming toxin
Monolayer
Supported lipid bilayer
Liquid-ordered phase
Liquid-disordered phase

ABSTRACT

α-Hemolysin (HlyA) is a protein toxin, a member of the pore-forming Repeat in Toxin (RTX) family, secreted by some pathogenic strands of *Escherichia coli*. The mechanism of action of this toxin seems to involve three stages that ultimately lead to cell lysis: binding, insertion, and oligomerization of the toxin within the membrane. Since the influence of phase segregation on HlyA binding and insertion in lipid membranes is not clearly understood, we explored at the meso- and nanoscale—both *in situ* and in *real-time*—the interaction of HlyA with lipid monolayers and bilayers. Our results demonstrate that HlyA could insert into monolayers of dioleoylphosphatidylcholine/sphingomyelin/cholesterol (DOPC/16:0SM/Cho) and DOPC/24:1SM/Cho. The time course for HlyA insertion was similar in both lipidic mixtures. HlyA insertion into DOPC/16:0SM/Cho monolayers, visualized by Brewster-angle microscopy (BAM), suggest an integration of the toxin into both the liquid-ordered and liquid-expanded phases. Atomic-force-microscopy imaging reported that phase boundaries favor the initial binding of the toxin, whereas after a longer time period the HlyA becomes localized into the liquid-disordered (*Ld*) phases of supported planar bilayers composed of DOPC/16:0SM/Cho. Our AFM images, however, showed that the HlyA interaction does not appear to match the general strategy described for other invasive proteins. We discuss these results in terms of the mechanism of action of HlyA.

1. Introduction

Pathogenic bacteria often secrete water-soluble protein toxins that can insert into cellular membranes and form aqueous pores. These toxins have the remarkable ability to change from a water-soluble state into one that inserts itself into a membrane as an oligomeric pore-forming complex. Many of these pore-forming peptides and proteins are critical pathogenic components and some are used for nanomedicine, sensing and nanoelectronic applications [1].

HlyA is an exotoxin that elicits a number of responses from a mammalian target cell to eventually alter the membrane permeability of that cell, causing lysis and death [2]. The synthesis, maturation, and secretion of *E. coli* HlyA are determined by the *hlyCABD* operon [3]. The gene-A product is a 110-kDa polypeptide corresponding to the protoxin (ProHlyA) that undergoes maturation to the active form (HlyA) within the bacterial cytosol through HlyC-directed acylation. This posttranslational modification involves a covalent amide linkage of fatty acids at two internal lysine residues (K563 and K689) that produces the activation [4]. The toxin is released from bacterial cells through a type I secretion mechanism [5] and, in the extracellular medium, HlyA must associate with calcium in order to bind to eukaryotic membranes in the lytically active form [6,7]. This second activation step is acylation-dependent since the calcium-binding capacity is lower in the unacylated protein [8]. HlyA lyses a wide range of host cells such as red blood cells, embryo and skin fibroblasts, granulocytes, lymphocytes, and macrophages [9]. HlyA can also bind to and disrupt protein-free liposomes [10].

The lytic activity of HlyA proceeds through a complex mechanism, and pore formation has been proposed to participate in the toxin's mechanism of cytolysis. Three stages seem to be involved that ultimately lead to cell lysis: binding, insertion, and oligomerization of the toxin in the membrane. The mechanism of HlyA insertion in lipid bilayers is not fully known; but as we have previously reported, the insertion is highly dependent on the physical properties of the bilayer [11]. In that work, experiments of HlyA insertion into bilayers formed by a variety

Abbreviations: HlyA, α-hemolysin; *Lo* phases, liquid-ordered; *Ld* phases, liquid-disordered; SM, sphingomyelin; BAM, Brewster-angle microscopy; AFM, atomic-force-microscopy; DRM, detergent-resistant membranes; 16:0SM, N-palmitoyl-D-erythro-sphingosylphosphorylcholine; 24:1SM, N-nervonoyl-D-erythro-sphingosylphosphorylcholine

* Corresponding author at: INIBIOLP, Facultad de Ciencias Médicas, 60 y 120, 1900 La Plata, Argentina. Tel.: +54 221 482 4894; fax: +54 221 4258988.
E-mail address: smate@med.unlp.edu.ar (S.M. Maté).

http://dx.doi.org/10.1016/j.bbamem.2014.02.022
0005-2736/

of single phospholipids, binary mixtures of phospholipids, or phospholipid and cholesterol, have revealed that insertion of the toxin into a membrane is favored by liquid-disordered (*Ld*) phases over either solid-ordered or liquid-ordered (*Lo*) phases. We have also reported that HlyA became associated with detergent-resistant membranes (DRM) enriched in sphingomyelin (SM) and cholesterol (Cho), isolated from sheep erythrocyte membranes [12]. Moreover, we found that when erythrocytes were depleted of Cho by methyl-β-cyclodextrin treatment, DRM-association, toxin oligomerization and hemolytic activity diminished, suggesting that membrane microdomains enriched in SM and Cho might be implicated in the oligomerization process.

Cho and SM have been proposed to interact *via* hydrogen bonding between the hydroxyl group of Cho and the amide group of the sphingosine and through hydrophobic interactions between the rigid Cho rings and the SM acyl chains. As a consequence of this differential interaction, *Lo* phases enriched in SM and Cho coexist with *Ld* phases in model membranes containing phosphatidylcholine (PC), SM, and Cho over a wide range of compositions [13]. Indeed, a similar situation is believed to occur in the plasma membrane of mammalian cells, where the preferential interactions of sphingolipids with Cho give rise to small domains of a transient nature known as lipid rafts [14]. The association of HlyA with detergent-resistant membranes enriched in SM and Cho seemed to contradict the above-mentioned preference of HlyA for irreversible insertion into *Ld* membranes. On the basis of these considerations we decided to investigate the influence of phase segregation on HlyA interaction with lipid membranes through the use of Brewster-angle microscopy (BAM) and atomic-force-microscopy (AFM) imaging.

As a first step in the study of HlyA–membrane interaction we examined the insertion of the toxin into lipid monolayers using BAM visualization. These lipid-monolayer studies enabled a scrutinization of the insertion step *per se* apart from the membrane lysis that would subsequently occur [15].

As the next step we examined the interaction of HlyA with lipid bilayers by AFM, which is a powerful tool for high-resolution imaging with nanometer resolution under physiological conditions to address key questions in biophysics and molecular microbiology that could not be answered by other techniques [16–18].

In this report we provide the first direct visualization of the interaction of HlyA with DOPC/SM/Cho monolayers and supported lipid bilayers that mimic the composition of red blood cell membranes [19–21]. Real-time AFM imaging demonstrated the occurrence of a preferential accumulation of the toxin into *Ld* phases rather than *Lo* phases, though lipid-packing defects arising at the interfaces between coexisting lipid phases function as initial binding sites for the toxin.

2. Material and methods

2.1. Materials

1,2-Dioleoyl-sn-glycero-3-phosphocholine (DOPC), N-palmitoyl-D-erythro-sphingosylphosphorylcholine (16:0SM), N-nervonoyl-D-erythro-sphingosylphosphorylcholine (24:1SM), and cholesterol (Cho) were purchased from Avanti Polar Lipids (Birmingham, AL, USA).

2.2. Protein purification

HlyA was purified from culture filtrates of *E. coli* strains WAM 1824 [22]. Cultures of the appropriate *E. coli* strain were grown to late log phase in Luria–Bertani medium to an optical density at 600 nm of 0.8–1.0 then pelleted and the supernatant was concentrated and partially purified by precipitation with cold 20% (v/v) aqueous ethanol at pH 4.5. The precipitate, containing the toxin, was collected by centrifugation at 14,500 ×*g* (1 h, 4 °C) and then resuspended in 20 mM Tris, 150 mM NaCl, 6 M urea, and pH 7.4 (TCU buffer). For further toxin purification the pellet obtained was loaded onto a Superdex 200 molecular-exclusion column (Amersham Biosciences) and the toxin eluted with TCU buffer. Sodium dodecyl sulfate-polyacrylamide gel electrophoresis (SDS-PAGE) analysis of this preparation showed a main band at 110 kDa corresponding to 95% of the total proteins in this sample (Fig. S1 in the Supplementary material). The protein was stored at −70 °C. Proteins were dialyzed in 20 mM Tris and 150 mM NaCl (TC buffer) (1:100 v/v) at 4 °C for 4 h before each experiment. The hemolytic activity of each stock of toxin purified was routinely checked as described Herlax et al. [23].

2.3. Surface-pressure measurements

Surface-pressure experiments were carried out with a NIMA Langmuir–Blodgett trough Model 102M (KSV-NIMA Biolin Scientific, Finland) with a Wilhelm platinum plate as surface-pressure sensor. The aqueous phase, or subphase, consisted of TC buffer containing 10 mM $CaCl_2$. The lipid, dissolved in chloroform:methanol (2:1), was gently spread over the surface of a Teflon microtrough containing only 200 μl of subphase until the desired initial surface pressure was attained (12 mN/m). The protein was injected with a micropipette into the subphase bulk. The increment in surface pressure *versus* time was recorded until a stable signal was obtained. All the experiments were carried out at a temperature of 20 °C. The figures show one of three closely similar independent measurements.

2.4. Surface-pressure-area isotherms

Compression isotherms were performed for Langmuir monolayers at a temperature of 20 °C. Stated in brief, a chloroform solution of lipid was spread onto the surface of a teflon trough filled with TC buffer with 10 mM $CaCl_2$ as the subphase. After solvent evaporation and relaxation at a $\pi \leq 0.1$ mN/m the film is compressed isometrically at a rate of 3 ± 1 Å$^2 \cdot$molec$^{-1} \cdot$min^{-1} to the target pressure. The parameter π was determined with a platinum plate by the Wilhelmy method. The equipment used was the KSV Microtrough (KSV NIMA_Biolin Scientific AB, Västra Frölunda, Sweden). In order to analyze the elastic behavior of the films, the compressibility modulus (C_s^{-1}) was calculated as follows [24]:

$$C_s^{-1} = -A\left(\frac{d\pi}{dA}\right)_T \quad (1)$$

where *A* represents the total monolayer area. For Langmuir isotherms, the $d\pi/dA$ data was obtained from regular compression experiments.

2.5. Brewster-angle-microscopy imaging

Film imaging by BAM was performed with an imaging ellipsometer (Nanofilm EP3sw imaging ellipsometer, Accurion GmbH, Germany) equipped with a 532 nm laser, a 20× objective, and a CCD camera operating at a resolution of 2 μm in the BAM mode. With an incident plane-polarized light, the equipment automatically finds the experimental Brewster angle of the subphase by measuring the intensity of reflected light at several angles of incidence and then performs a calibration of the reflected light and the gray-level intensity measured by the CCD camera.

Insertion experiments at constant surface pressure and 20 °C were conducted in a KSV minitrough equipment (KSV-NIMA Biolin Scientific, Finland) mounted on the stage of an Accurion elipsometer. The working portion of subphase of the rectangular compartment (200 ml, 7.5 cm × 21.5 cm) was restricted to the area inside a cylindrical glass ring (10 ml volume) that communicated with the rest of the trough through indentations in the upper edge of the cylinder's etched glass (3 mm wide and less than 1 mm deep). The BAM imaging was carried within the cylindrical compartment. The two surface-connected compartments were filled with TC buffer

containing 10 mM $CaCl_2$, and a lipid monolayer was deposited onto the aqueous surface to the desired pressure. After surface-pressure stabilization (5 min) an aliquot of HlyA was injected into the subphase of the smaller compartment under continuous stirring, and the monolayer area was automatically adjusted in order to maintain the surface pressure constant over time. This experimental design allowed us to reduce the amount of protein needed since only the monolayer diffuses through the narrow surface canal, thus minimizing the mixing of the subphase of the two compartments.

The public software ImageJ (1.43u, Wayne Rasband, National Institutes of Health, Bethesda, MD) was used for the gray-level determination on the raw data obtained by BAM. For a better visualization, the lower 0–100 gray level range (from the 0–255 original scale) was selected. The figures are representative of three independent experiments.

2.6. Multilamellar-vesicle preparation

Multilamellar vesicles were prepared by mixing the appropriate amount of synthetic pure lipids (16:0SM or 24:1SM; DOPC and Cho) dissolved in chloroform/methanol (2:1, v/v). The samples were dried by evaporating the solvent under a stream of nitrogen and then placing them at high vacuum for 2 h in a glass chamber connected to a vacuum pump. The samples were hydrated in 25 mM HEPES, 150 mM NaCl, and pH 7.4 (assay buffer) with stirring to facilitate dispersion.

2.7. Formation of supported lipid bilayers

Supported lipid bilayer preparations on mica substrates for AFM measurements were performed by means of the vesicle-fusion technique [25]. Multilayered vesicles prepared as described previously were introduced into an FB-15049 (Fisher Scientific Inc., Waltham, MA, USA) bath sonicator and treated with ultrasound at 65 °C for 1 h to generate small unilamellar vesicles. Next, 120 μl of assay buffer containing 3 mM $CaCl_2$ were added onto a 1.2-cm^2 freshly cleaved mica substrate attached to a steel disk for placement in the liquid cell to be used for atomic-force-microscopy measurements (Nanoscope V&Multimode, Veeco, USA). Small unilamellar vesicles (60 μl) in assay buffer were deposited onto the mica disk and were incubated at 65 °C for 60 min in the presence of a water reservoir to prevent evaporation from the sample. Final lipid concentration was 150 μM. After the samples were left for a further 60 min at room temperature, the nonadsorbed vesicles were discarded by washing the samples 10 times with assay buffer in the absence of $CaCl_2$. A small amount of buffer was always left on top of the substrate in order to maintain the supported lipid bilayers hydrated at all times.

2.8. Atomic force microscopy imaging

AFM measurements were performed on a multimode atomic-force microscope controlled by a Nanoscope-V unit (Veeco, USA). NP10 silicon-nitride probes (Veeco Instruments Inc., USA) with a spring constant of 0.12 and/or 0.35 N/m were used in contact-mode scanning in the fluid cell to measure the supported lipid bilayers, while the minimum possible force was continuously maintained. All the experiments were carried out at a temperature of 24 °C. Resolution images of 512 × 512 pixels were collected at a scanning rate between 1 and 1.5 Hz. The height and error-signal (vertical deflection) images were taken simultaneously. HlyA (50 μl of a 0.2 μg/μl suspension in assay buffer containing 3 mM $CaCl_2$) was immediately added to the fluid cell, and the sample was imaged again in order to obtain reference images of the membrane-associated protein. The sequence of images shown in Figs. 6 and 8 corresponds to a single experiment that is representative of three independent measurements.

3. Results

The present study has examined the influence of phase segregation on HlyA binding and insertion into lipid membranes. Since we recently found that HlyA associates with detergent-resistant membranes isolated from sheep erythrocytes, we have inferred that membrane microdomains enriched in SM and Cho act as platforms for the concentration of toxin as an essential step in oligomerization [12]. We therefore performed experiments of HlyA interaction with monolayers and bilayers of DOPC/16:0SM/Cho and DOPC/24:1SM/Cho (each in a 2:1:1, molar ratio) since these lipid mixtures exhibit differences in phase-separation behavior (*cf.* below). We have chosen to compare the well known DOPC/16:0SM/Cho mixture [26,27] with the so far unexplored ternary mixture containing 24:1SM since sheep erythrocyte membranes and respective detergent-resistant fractions contain high proportions of this SM molecular specie [28]. Furthermore, while $24{:}1^{\Delta 15}$ has recently been recognized as a common N-linked acyl chain in natural SMs [29,30] only few studies have addressed the interaction of this lipid with the neighboring lipids in domain formation [31,32].

3.1. Characterization of ternary monolayers

Lipid monolayers at the air–water interface represent the most simplified reconstitution model for simulating biologic membranes. Pure 16:0SM-containing monolayers show a *Le* (liquid-expanded)–*Lc* (liquid-condensed) phase transition at 13 mN/m at 20 °C indicated by a quasi-plateau in the surface pressure (π)–molecular area plot (Fig. 1A), whereas 24:1SM monolayers were characterized by a *Le* behavior over the entire surface-pressure range up to collapse (Fig. 1 A). These observations were consistent with the results reported by Li et al. [33]. This different behavior can be observed in compression-isotherm experiments of the pure components and their corresponding compressibility modulus (C_s^{-1}) (Fig. 1A and C), whose typical values are ~100 mN/m or lower for *Le* phases but above this figure for *Lc* (and *Lo*) phases.

When 16:0SM is mixed with a short or unsaturated phosphatidylcholine and Cho, a two-phase system is established in both monolayers and bilayers [27,34]. DOPC monolayers behave as *Le* films, as evidenced by the low C_s^{-1} values obtained (*cf.* Fig. 1A and C). This property is what determines that PC will become the main component of the *Le* phase in the ternary monolayer, while the *Lo* properties of pure Cho monolayers become extended to the SM- and Cho-enriched *Lo* phase in the ternary mixture [27]. The isotherm of the ternary monolayer containing 16:0SM shows a smooth *Le*-like behavior (Fig. 1B and D). Since the π of a monolayer is a macroscopic property, the isotherm gives the average information for the film (such as the average area per molecule) along with its rheological properties (*i.e.*, C_s^{-1}), but cannot assess the texture of the film. In order to inspect this property we performed BAM experiments on the ternary films.

BAM visualization of 16:0SM-containing lipid mixtures reveals phase coexistence with a thick phase (light gray) forming circular domains immersed in a thinner phase (dark gray), until a π of 25 mN/m is exceeded, at which point both phases merge (Fig. 2A). Previous results by Fanani et al. [27], involving DLPC/16:0SM/Cho monolayers, supports the assignment of an *Lo* character to the thick phase and *Le* character to the thinner continuous phase.

We also investigated the as-yet-unreported DOPC/24:1SM/Cho ternary monolayer. The compression isotherm of this mixture (Fig. 1B)—similar to that of the 16:0SM containing monolayer—showed a smooth expanded profile but over a somewhat larger mean molecular area throughout the whole surface-pressure range along with slightly lower C_s^{-1} values (Fig. 1D). This behavior may be due to a stronger condensation effect for the ternary 16:0SM film than for the 24:1SM film which is typically found in phospholipid/Cho mixed monolayers and constituting a principal characteristic of the *Lo* phase in those monolayers [35]. Visual inspection of the 24:1SM ternary monolayer by BAM (Fig. 2B) revealed that *Lo* domains were present only at low π

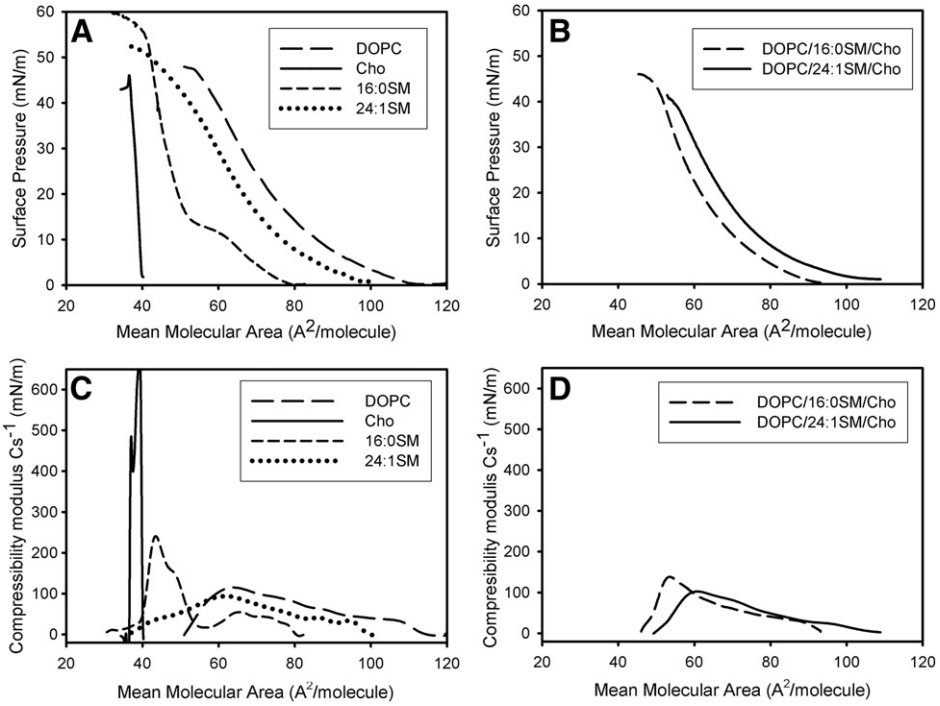

Fig. 1. Characterization of ternary monolayers. Surface-pressure–area isotherms of (A) pure lipids and (B) ternary lipid mixtures. (C and D) Compressibility moduli (C_s^{-1}) corresponding to each isotherm. Lipids used were: DOPC (long dash line), 16:0SM (short dash line), 24:1SM (dotted line) and Cho (solid line) in (A) and (C). Ternary lipid mixtures composed of DOPC/16:0SM/Cho (medium dash line) and DOPC/24:1SM/Cho (solid line; both in 2:1:1 mol ratio) in (B) and (D). The experiments were performed at 20 °C.

(<4 mN/m). This result may indicate a poor stabilization of the *Lo* domain (and accordingly the domain borders) by this unsaturated SM so that merging requires less compression to occur.

From the above characterization of our ternary lipid mixtures we concluded that the isotherms of both mixtures showed that the overall behavior of the films is quite similar and, therefore comparable in thermodynamic terms, which comparison is informative at a macroscopic level. However, the microscopic organization and texture of the ternary films differ, as reported by BAM experiments. Thus, besides general thermodynamic similitude, in the surface-

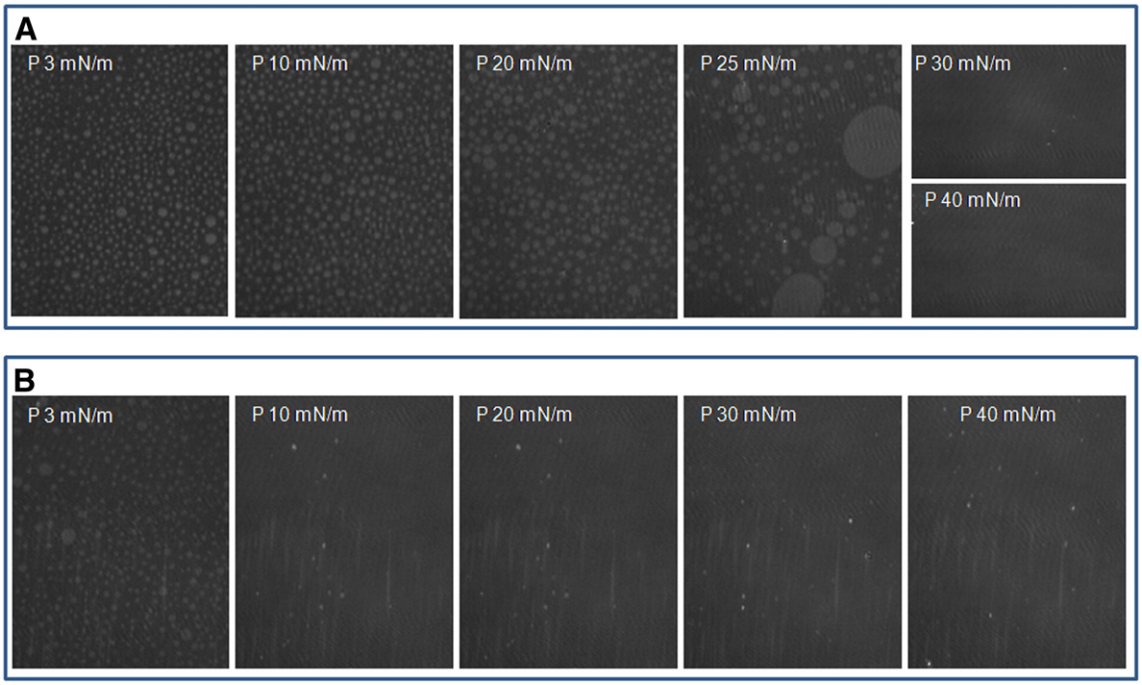

Fig. 2. BAM images of DOPC/SM/Cho monolayers during compression. BAM visualization of ternary mixtures containing (A) DOPC/16:0SM/Cho and (B) DOPC/24:1SM/Cho. Photographs were taken at the surface pressures indicated in each image. For better visualization the lower 0–100 gray level range (from 0 to 255 in the original scale) was selected in order to keep the relationship between gray level and film thickness comparable. The experiments were performed at 20 °C. Images are representative of three independent experiments.

pressure range of 10–25 mN/m, only the 16:0SM-containing ternary mixture exhibited phase coexistence. Then, we further explored if this difference is sensed by the toxin adsorption to the lipid film.

3.2. Monolayer insertion of HlyA

As a first step in the study of HlyA interaction with the above-described model membranes, we undertook adsorption experiments. Fig. 3A shows the time course of adsorption of HlyA onto the air–water interface. Injection of HlyA into the aqueous subphase led to an increase in the π in a dose-dependent manner, as a result of the surface-active properties of HlyA, as had been previously reported by Sanchez-Magraner et al. [15]. At the lowest toxin concentration assayed (40 nM) a lag phase in the surface-pressure increase was observed. This interval became shorter with an increasing toxin concentration and became no longer detectable at 160 nM HlyA.

Fig. 3B shows the insertion of HlyA into monolayers at the air–water interface composed of DOPC/16:0SM/Cho or DOPC/24:1SM/Cho. The time course of HlyA insertion and the total increment of 10 mN/m in the π after 40 min (2400 s) were very similar in both ternary lipid mixtures.

The surface morphology of the insertion events was monitored by BAM which allows a determination of the influence of phase separation (optical thickness and surface topography) on HlyA insertion. The monolayers were compressed to a π of 20 mN/m and, after HlyA injection, the changes in film morphology over time were monitored. In the following Figs. 4 and 5 we show the images corresponding to the first 10 min after HlyA injection into the subphase because, as we mentioned in Section 2.5, the working portion of the subphase was restricted allowing us to reduce the amount of toxin needed but the monolayer diffusion along the entire compartment not being restricted. Then, we recorded only the initial changes in film morphology under the microscope focus point (from 0 to 10 min after toxin injection). HlyA insertion into a monolayer composed of DOPC/16:0SM/Cho did not cause domain coalescence, but rather the mean gray intensity increased in both phases of this ternary-lipid mixture (Fig. 4). The mean gray intensity (over the background) increased from 12.3 ± 0.08 to 14.0 ± 0.88 (14%) and from 6.5 ± 0.03 to 8.9 ± 0.71 (36%) for the *Lo* and *Le* phases,

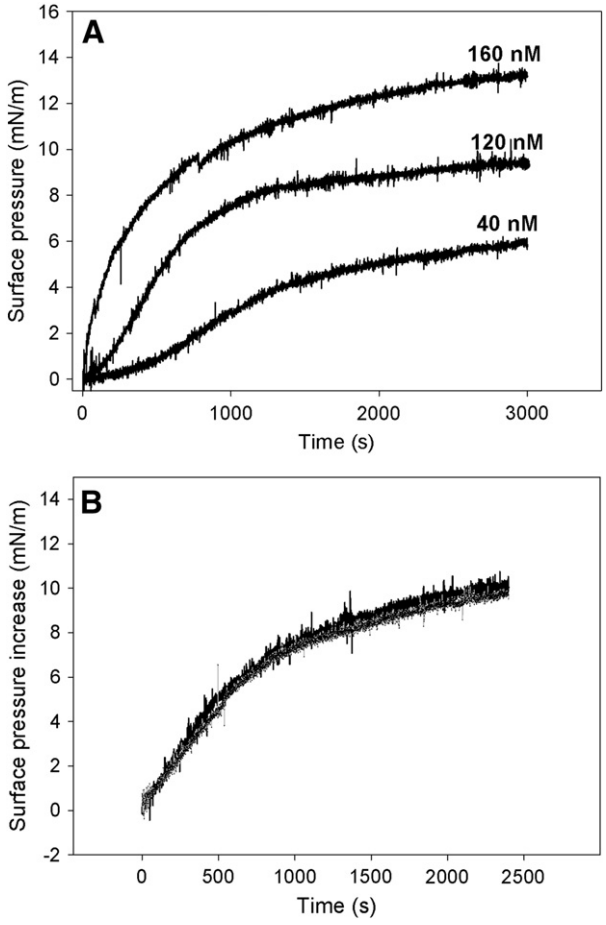

Fig. 3. HlyA insertion into DOPC/SM/Cho monolayers. (A) Time course of the adsorption of HlyA at an air–water interface, measured with a Langmuir trough at 20 °C. The subphase composition was 20 mM Tris–HCl, 150 mM NaCl, 10 mM $CaCl_2$, pH 7.4. The protein concentration is indicated for each curve. (B) Time course of the insertion of HlyA into lipid monolayers at an initial lateral pressure of 12 mN/m at 20 °C. The experiments were performed in the presence of a subphase with the same composition as described in A. The lipid component was DOPC/16:0SM/Cho (black line) and DOPC/24:1SM/Cho (gray line; both in a 2:1:1 mol ratio). The initial protein concentration in the subphase was 120 nM.

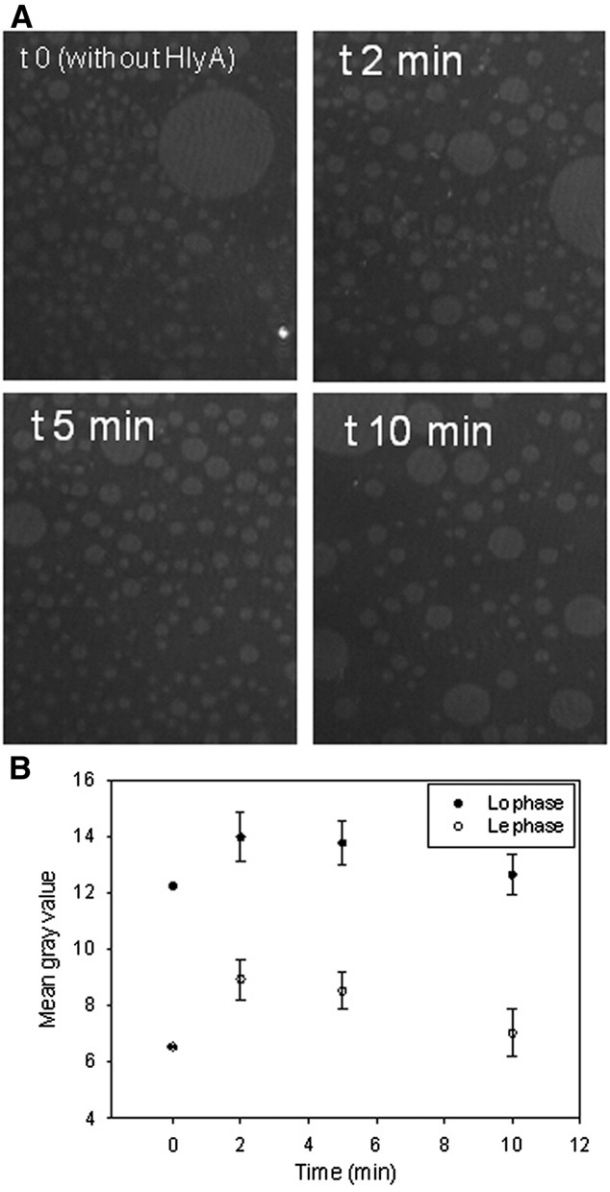

Fig. 4. BAM images of the time course of the insertion of HlyA into a lipid monolayer of DOPC/16:0SM/Cho at an initial lateral pressure of 20 mN/m at 20 °C. (A) The subphase composition was 20 mM Tris–HCl, 150 mM NaCl, 10 mM $CaCl_2$, pH 7.4. The window intensities of the BAM images shown were scaled from 0–250 to 0–100 in order to enhance visualization of the domain borders. The initial protein concentration in the subphase was 120 nM. (B) Evolution of the changes in mean gray value over time within the two phases. The values are means ± SEM from a set of three independent experiments and at least ten different regions of the same phase were analyzed in each image. When no error bar is observed, the corresponding SEM value is smaller than the size of the point.

respectively, after 2 min of HlyA injection into the subphase (Fig. 4B). Since the value of gray intensity in the BAM experiments depends on both the refractive index and the thickness of the film, the increase observed in that measurement implies that a change in either or both of those parameters has occurred. Because the increase of the film thickness due to the insertion of HlyA has been reported previously [36], an integration of the toxin into the *Lo* as well as the *Le* phase can be suggested—but not necessarily in the same proportion—which is noticeable.

Fig. 5A shows the surface topography of DOPC/24:1SM/Cho as visualized by BAM after HlyA addition to the subphase. As described above, this ternary-lipid mixture showed no phase coexistences at π higher than 4 mN/m. HlyA insertion furthermore induced no phase separation, and the mean gray value of the unique phase increased 36% (from 3.3 ± 0.19 to 4.5 ± 0.72), thus producing the same effect as *Le* phase in mixture with 16:0SM (Fig. 5B).

3.3. AFM imaging of HlyA interaction with supported lipid bilayers

The results obtained from the BAM imaging of the HlyA insertion suggested that lipid-phase coexistence had no effect on HlyA membrane insertion and thus HlyA could penetrate both the *Lo* and *Le* phases. In order to investigate thoroughly the influence of phase segregation on HlyA interaction with lipid bilayers, we performed AFM experiments that would provide a resolution of the phenomenon within the nanometer scale. Supported lipid bilayers (SLBs) were prepared with the same lipids used in the monolayer experiments by the fusion of small unilamellar vesicles on freshly cleaved mica. The interaction of HlyA with these lipid bilayers was then imaged *in situ* by AFM in a buffer containing Ca^{+2} because HlyA needs calcium in order to bind to membranes in the lytically active form [6,7].

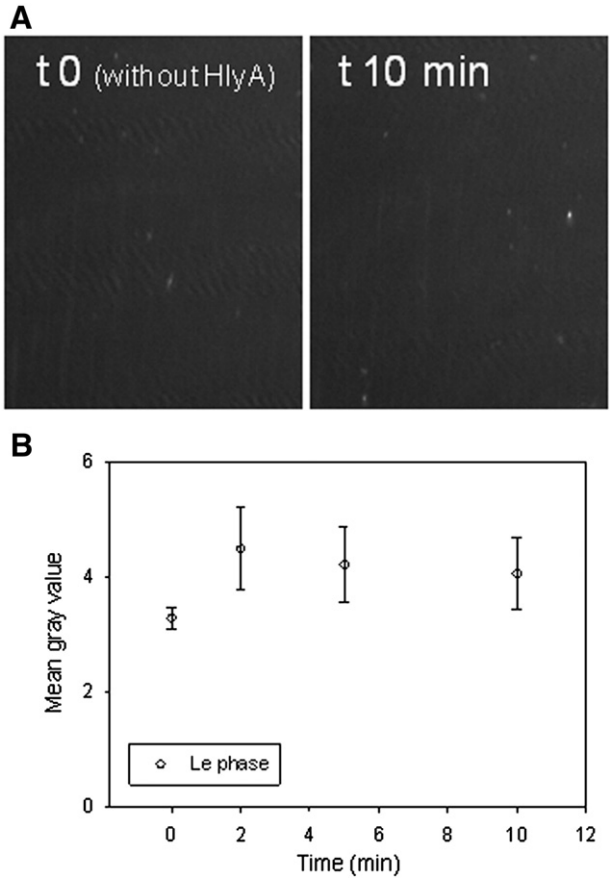

Fig. 5. BAM images of the time course of the insertion of HlyA into a lipid monolayer of DOPC/24:1SM/Cho at an initial lateral pressure of 20 mN/m at 20 °C. (A) The subphase composition was 20 mM Tris–HCl, 150 mM NaCl, 10 mM $CaCl_2$, pH 7.4. The window intensities of the BAM images shown were scaled from 0–250 to 0–100 in order to enhance visualization of the domain borders. The initial protein concentration in the subphase was 120 nM. (B) Evolution of the changes in mean gray value over time for the uniform *Le* phase observed. The values are means ± SEM from a set of three independent experiments and at least ten different regions of the same phase were analyzed in each image. When no error bar is observed, the corresponding SEM value is smaller than the size of the point.

Fig. 6 shows, in real time, a SLB composed of DOPC/16:0SM/Cho without HlyA present (Fig. 6A) and during the interaction with the toxin (Fig. 6B–D). In good agreement with the BAM images, this lipid mixture exhibits a clear phase separation, with a *Lo* phase (SM/Cho-enriched) protruding 1.06 ± 0.06 nm from the darker continuous *Ld* phase (related to the *Le* phase in monolayers)—*i.e.*, the DOPC-enriched matrix (see Fig. S2 in Supplementary material). Scans of this DOPC/16:0SM/Cho SLB in the absence of HlyA, and performed in a buffer containing $CaCl_2$, revealed that the shape of the *Lo* domains did not vary between successive scans of the same zone, even after prolonged scanning (for more than 2 h, data not shown). The image in Fig. 6B, indicated as *Start*, was obtained immediately after HlyA addition. Here, as visualized in *real-time*, HlyA initially binds at the periphery of the *Lo* domains. The imaging at a higher magnification confirmed that the increase in height of the boundary between the domains could be attributable to the binding of HlyA—it appearing as bright dots (Fig. 6C). The protrusion of HlyA, measured from the surface of the bilayer to the top of the protein by AFM, was 10 ± 0.7 nm (*cf.* line profile in Fig. 6). The scan of the same zone in the SLB after 45 min of HlyA incubation accordingly shows a time-dependent accumulation of the HlyA preferentially into the *Ld* phase (Fig. 6, images D–F). A significant observation here was that the shape of the *Lo* domains did not change over time. Of interest too was that the AFM images indicated that the initial binding of HlyA into the boundary of the *Lo* domains occurred along with lipid rearrangement and the formation of defects appearing in the form of black spaces within the *Lo* domains (Image B in Fig. 7). The line profile in Fig. 7 shows that the depth of the defects was *ca.* 1 nm (Fig. 7C) and that the height difference between the *Ld* and the *Lo* phases was not modified by HlyA binding (Fig. 7D).

Fig. 8 shows the interaction of HlyA with a DOPC/24:1SM/Cho (2:1:1 molar ratio) SLB. The procedure for the assembling of the supported lipid bilayer allows the formation of bilayers completely covering the mica substrate. As visualized by AFM, the DOPC/24:1SM/Cho bilayers appear to be uniformly flat and, in agreement with the previous examination of the monolayers by BAM, the AFM images of this SLB showed no phase separation. After HlyA addition the imaging *in situ* by AFM revealed that the toxin was homogeneously bounded to this ternary lipid mixture, with a HlyA protrusion of 7 ± 0.7 nm occurring from the surface of the bilayer (*cf.* the line profile in Fig. 8). We have made control experiments with bare mica modified with Ca^{2+} ions (this procedure was used to promote vesicle fusion in DOPC/24:1SM/Cho SLB formation). The image (Fig. S3 left side, in Supplementary material) shows a completely smooth surface which is quite different from that shown in Fig. 8A, where a homogeneous bilayer film is on mica. The image obtained when HlyA is added in the fluid cell on mica modified with Ca^{2+} ions is shown in Fig S3, right side, in Supplementary material. The continuous scanning of the sample produces cord-like forms where the AFM probe tends to sweep away these weakly bound proteins. These effects are not observed under similar experimental conditions when the HlyA is added to DOPC/24:1SM/Cho lipid bilayers supported on mica.

4. Discussion

Attempts to visualize membrane heterogeneity directly in live cells have thus far remained unsuccessful by conventional microscopy. Phase-separated monolayers and SLBs have been widely used as simple model systems for studying membrane heterogeneity [13,18,37]. Because of the capacity to image structures in aqueous media with a resolution that extends from the microscopic to the molecular level, AFM

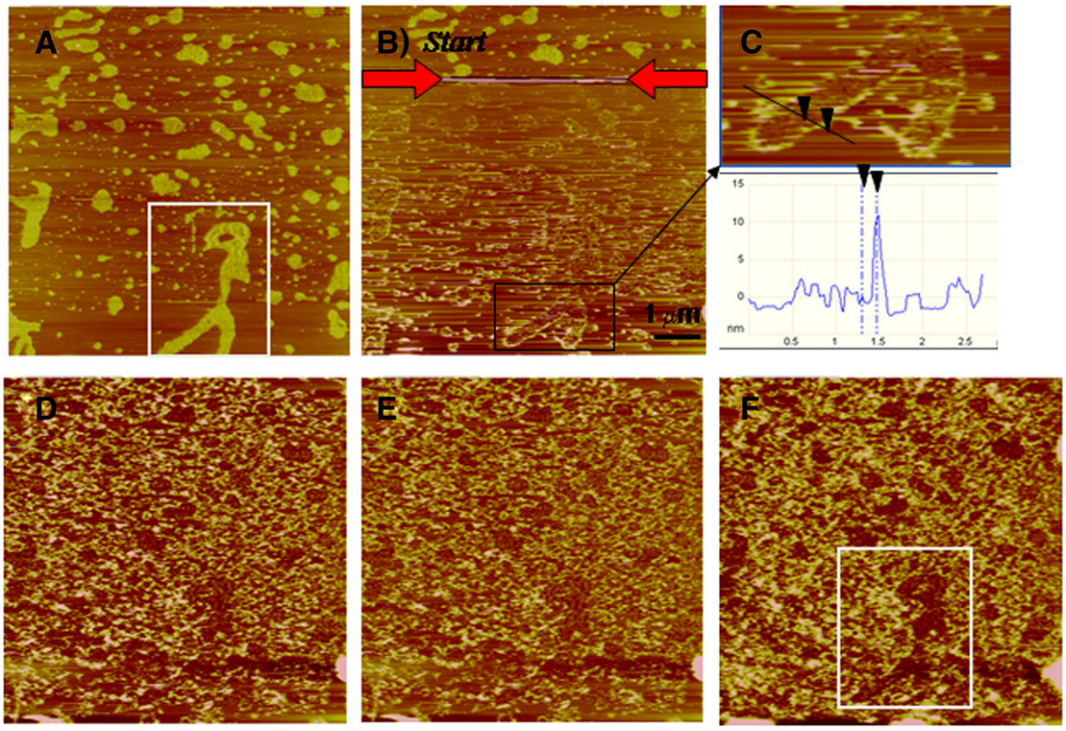

Fig. 6. AFM topographical images of a supported lipid bilayer composed of DOPC/16:0SM/Cho (2:1:1, mol ratio) in assay buffer containing 3 mM $CaCl_2$. (A) The supported lipid bilayer without HlyA addition. (B) The same supported bilayer as in A, but immediately after addition of HlyA. (C) Cross-section profile of image in panel B. (D–F) Images D, E and F were captured after HlyA addition by sequential scans over the same area of the sample. The time elapsed at the end of each scan was (D) 15 min, (E) 30 min, and (F) 45 min. The scale bar is indicated in (B).

microscopy has become a useful tool for investigating membrane microdomains as well as for exploring the adsorption of water-soluble protein toxins to, or their association with, lipid bilayers [18,38,39]. In this work we have combined monolayer (along with BAM imaging) and bilayer (*in-situ* AFM imaging) approaches to examine the influence of phase separation on HlyA interaction with membranes.

Lipid monolayers are extremely useful for studying lipid–protein interactions because those model membranes permit the control of several physical parameters—*e.g.*, the surface pressure and lipid density along with the subphase content and lipid composition. Since the aim was to study the influence of phase separation on the interaction of HlyA with monolayers, we had to work at a surface pressure below 25 mN/m, in order to observe differences in phase behavior between monolayers (Fig. 2), although the surface pressure of biological membranes is in the range of 30–35 mN/m [40–42]. This pressure also falls within the range that is more sensitive to the toxin penetration. HlyA insertion into this membrane model allowed us the direct observation of the insertion phenomenon separated from further changes in the lipid architecture because, by its very design, the monolayer could not undergo the three-dimensional membrane restructuring that would be essential for altering the membrane-permeability barrier. Thus, the lipid-monolayer studies enabled a scrutinization of the insertion step *per se* apart from the membrane lysis that would subsequently occur [15].

The BAM experiments indicated that the microscopic organization and texture of the DOPC/16:0SM/Cho and DOPC/24:1SM/Cho films differed and that, despite general thermodynamic similarity between the

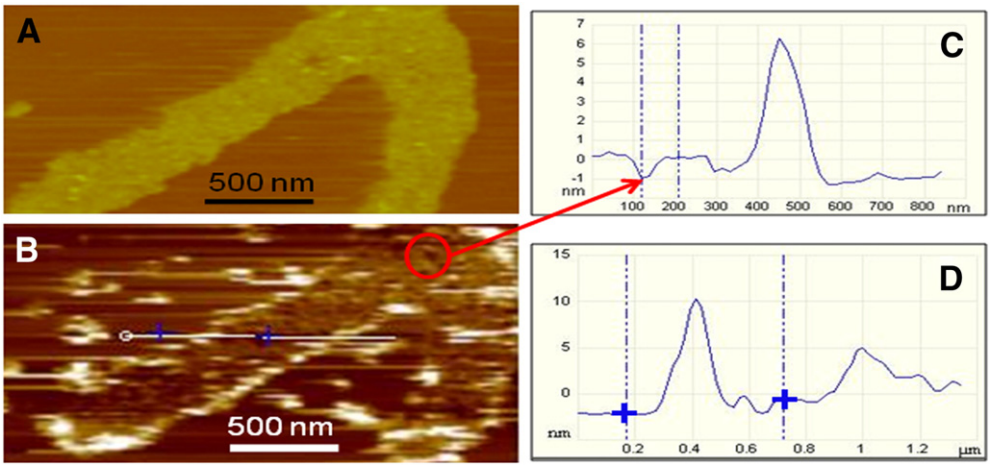

Fig. 7. HlyA binding to the boundary of *Lo* domains on supported lipid bilayers composed of DOPC/16:0SM/Cho. (A) The supported lipid bilayer without HlyA addition. (B) The supported lipid bilayer after HlyA addition. Scale bar: 500 nm. (C) Cross-section profile of a defect encircled in red (D) Cross-section profile showing height difference between the *Ld* phase and the *Lo* domains.

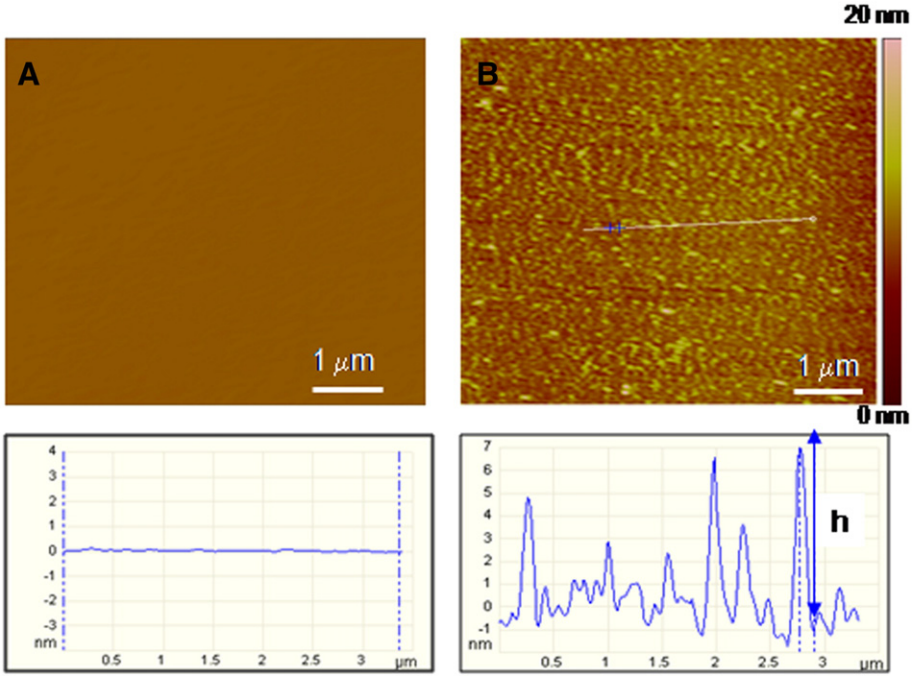

Fig. 8. AFM topographical images of a supported lipid bilayer composed of DOPC/24:1SM/Cho (2:1:1, mol ratio) in assay buffer containing 3 mM $CaCl_2$. Images from 0 to 45 min were photographed by sequential scans over the same area of the sample. (A) The supported lipid bilayer without HlyA addition. (B) The supported lipid bilayer after 45 min of interaction with HlyA. Scale bar: 1 μm. Cross-sectional line profiles are shown below each image. Color scale bar at the right side provides z-range.

two films, within the surface-pressure range of 10–25 mN/m, only the 16:0SM-containing ternary mixture manifested coexistence of *Lo* and *Le* phases. The insertion of HlyA into either monolayer exhibited the same kinetics (Fig. 3), leading to a total change in lateral pressure ($\Delta\pi$) of 10 mN/m. This result is in agreement with the findings of Sánchez-Magraner et al., although those authors used a different lipid mixture (*i.e.*, egg PC, egg phosphatidylethanolamine, and Cho at a 2:1:1 mol ratio) [15]. From the present insertion experiments with monolayers we can conclude that from a macroscopic point of view lipid-phase coexistence does not favor HlyA membrane insertion. BAM imaging, in a mesoscopic analysis, showed that HlyA insertion causes changes in the mean gray value of both phases in the DOPC/16:0SM/Cho monolayer, probably indicating that toxin insertion takes place in both phases of this ternary lipid mixture or that the insertion in one phase produces changes also in the other phase. This result suggests that during the first 10 min of HlyA interaction with the monolayers, and on a micrometer scale, the toxin exhibits no notable preference for any phase. One should keep in mind that the changes in gray level of the *Lo* and *Le* phases may not be equally reflective of the amount of the inserted protein.

In order to test the interaction of the toxin with membranes under conditions similar to those found in biomembranes, where the differences in packing density between the *Lo* and *Ld* phases are much larger than those between the two phases in our monolayer assays, we performed AFM experiments in supported bilayers having the same lipid composition as the monolayers. Importantly, as we cannot be absolutely sure that we are observing the insertion of the toxin, we use the term "binding" instead of "insertion" for AFM results.

The AFM imaging of SLBs composed of DOPC/16:0SM/Cho (2:1:1, molar ratio) exhibited numerous *Lo* domains that were thicker than the surrounding disordered phase, with a difference in height between the two phases of *ca.* 1 nm. These measured height differences were in good agreement with Sullan et al., who reported a height difference between those two phases of 0.8–1.2 nm in 10–35% and 0.6 nm in 40% Cho [13]. A further aspect that deserves some comment is the difference in morphology observed for *Lo* domains between a monolayer and SLBs. Morphology of domains in monolayers has been well established to depend on competition between two opposing effects—namely, line tension at the domain borders and perpendicular dipole–dipole repulsion between coexisting phases, according to McConnell's shape-transition theory [43]. Therefore, the circular shape observed for *Lo* domains in monolayers indicated that line tension is the dominant parameter. In contrast, for supported lipid bilayers, domain nucleation and growth are highly dependent on the thermal history of the sample [44,45] and thus, rather than being in equilibrium, may be kinetically restricted through a loss of mobility produced by a strong interaction with the solid support. Therefore, the shape of the *Lo* domains varied considerably, both within a given sample and from sample to sample, and may be either rounded or elongated [46].

In contrast with the ternary-lipid mixture containing 16:0SM—and in agreement with the BAM analysis of the monolayers—the AFM imaging confirmed the presence of a uniform lipid distribution in the SLBs composed of DOPC/24:1SM/Cho (Fig. 8). This result suggested that SMs with a very long and unsaturated N-linked acyl chain had poor tight-packing propensities with which to stabilize ordered-domain formation by interaction with cholesterol. This conclusion is consistent with the results of confocal microscopy that indicated the absence of phase separation in giant unilamellar vesicles prepared with POPC/24:1SM/Cho (at a 60:30:10, molar ratio) [32].

The AFM scan of the SLBs composed of DOPC/16:0SM/Cho that were incubated with HlyA revealed a preferential accumulation of the toxin into the *Ld* over the *Lo* phase at longer time scales; but most significantly, as mentioned above, the lipid packing defects arising at the interfaces between the coexisting phases function as initial binding sites for the toxin. AFM and crystallography studies on model membranes had demonstrated that the *Lo* phase was thicker than the *Ld* phase as a result of the higher conformational order of the acyl tails [47]. To avoid the exposure of the hydrophobic side chains to the aqueous solvent, the lipids were found to bend elastically at the domain interface, causing a curvature stress with a concomitant energetic cost per unit length or line tension [48]. As a consequence, the concentration of packing defects at the phase boundaries was higher. In a recent article Sheikh et al. [46] characterized by AFM the hydration features of the model lipid raft boundary region. The authors imaged a thin intermediate bilayer

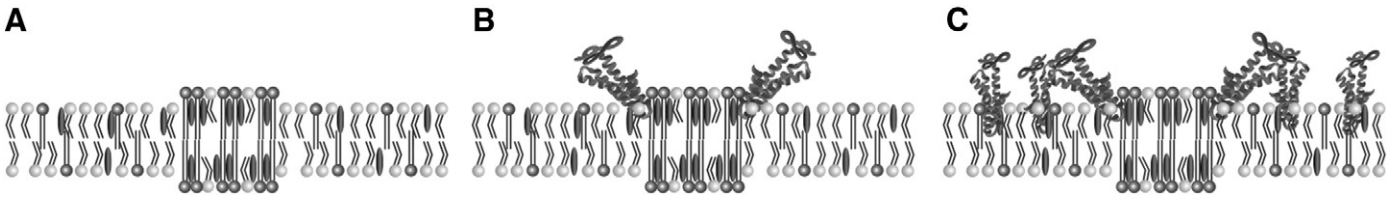

Fig. 9. Schematic model for the binding of HlyA to membranes exhibiting phase segregation. (A) A lipid mixture exhibiting phase separation between *Lo* (higher) domains, surrounded by a *Ld* (lower) phase. In the figure, the *Ld* phase is represented by lipids with light gray headgroups and disordered acyl chains, the *Lo* phase is represented by SM molecules with dark gray headgroups and extended acyl chains, and the Cho molecules are represented by ellipses. (B) HlyA initially binds at domain boundaries through the amphipathic α-helical regions of the proteins present. Localization of HlyA in the interfaces will provide a vehicle for lipid–protein associations which leads to the stabilization of domain borders. (C) A further interaction of HlyA occurs in the *Le* phase.

between the coexisting lipid phases that did not have detectable hydration layers and suggested that the domain boundaries would present more energetically favorable regions for interactions with external biomolecules. Indeed, several examples of toxins that localize at domain boundaries have been reported [49,50]. Very recently, Ros et al. [21] reported that the sticholysin family of pore-forming toxins reduces line tension in DOPC/SM/Cho membranes by promoting lipid mixing. The authors showed by AFM that the toxins adsorbed in the *Ld* phase promoted a reduction in line tension between the *Lo* and *Ld* phases, as evidenced both by a decrease in the phase–height difference and by changes in domain shape. In fact, in a study of the proapoptotic protein Bax, García-Sáez et al. [47] proposed that a decrease in line tension may be a general strategy of invasive pore-forming peptides and proteins.

That AFM images in the present work revealed that HlyA binding to domain boundaries did not cause membrane thickening or any change in the morphology of the *Lo* domains is indeed striking. Interactions between lipids and membrane proteins are necessarily of a high degree of complexity. The essential question as to whether a specific interaction or only a small number of interactions dominate has not yet been explored [51]. The overall objectives of such protein–lipid studies would include finding the energy of the protein interaction with each type of lipid in a mixture and also the number of energetically significant interactions of the protein with different neighboring lipids. Only then may a feasible explanation of the striking HlyA behavior be in the offing since the HlyA interaction does not appear to match the general strategy described for other invasive proteins, but rather seems to be related to the HlyA size and structure; which characteristics, in fact, produce a paradoxical lipid dependence on the toroidal pores formed by the toxin. Bakas et al. reported that, in contrast to the expectation, HlyA-induced pores were stabilized by lipids inducers of negative curvature that for other membranolitic toxins lead to the opposite effects [36]. The dependence of HlyA pores on lipid composition in planar lipid bilayers is consistent with the data on liposome permeability. PE and cholesterol promote high leakage in the presence of HlyA [10]. Furthermore, LPC, a positive curvature inducer, also neutralized the lytic activity promoted by PE in liposomes [10]. The localization and accumulation of HlyA in the domain interfaces likely provide a vehicle for lipid–protein associations that lead to no changes in domain pattern. This mechanism could explain the absence of lipid mixing and the constancy of domain morphology observed.

5. Conclusions

Binding to membrane defects may represent a common mechanism of action for membranolitic proteins, rendering insertion and stabilization of an open-pore state energetically favorable. It was postulated that proteins and peptides preferentially bind to lipid packing defects arising at the interfaces between the coexisting phases, reducing line tension and leading to domain dispersion [52]. Our AFM images, however, showed that the HlyA interaction does not appear to match the general strategy described for other invasive proteins. The results presented in this paper constitute another example of how the mechanism of action of large proteins such as HlyA may differ from the interactions of small molecules. On the basis of the obtained data, we feel tempted to propose here a schematic model depicting HlyA interaction within the lipid bilayers that exhibited phase separation (Fig. 9).

Acknowledgements

This work was supported by grants from the Comisión de Investigaciones Científicas de la Provincia de Buenos Aires, and Agencia Nacional de Promoción Científica y Tecnológica Grant PICT Nos. 2129 and PICT-CNPQ-0019. SMM, MEV and LSB are researchers from CIC PBA. SMM, VH, RV and LSB are members of the Iberoamerican CYTED Network BIOTOX 212RT 0467. The authors thank Mario Ramos for the graphic designs.

Appendix A. Supplementary data

Details of toxin purification and AFM images are available as supplementary material. Supplementary data to this article can be found online at http://dx.doi.org/10.1016/j.bbamem.2014.02.022

References

[1] S. Majd, E.C. Yusko, Y.N. Billeh, M.X. Macrae, J. Yang, M. Mayer, Applications of biological pores in nanomedicine, sensing, and nanoelectronics, Curr. Opin. Biotechnol. 21 (2010) 439–476.
[2] T.J. Wiles, M.A. Mulvey, The RTX pore-forming toxin α-hemolysin of uropathogenic *Escherichia coli*, Future Microbiol. 8 (2013) 73–84.
[3] R.A. Welch, RTX toxin structure and function: a story of numerous anomalies and few analogies in toxin biology, Curr. Top. Microbiol. Immunol. 257 (2001) 85–111.
[4] P. Stanley, V. Koronakis, C. Hughes, Acylation of *Escherichia coli* hemolysin: a unique protein lipidation mechanism underlying toxin function, Microbiol. Mol. Biol. Rev. 62 (1998) 309–333.
[5] I. Linhartová, L. Bumba, J. Mašín, M. Basler, R. Osička, J. Kamanová, K. Procházková, I. Adkins, J. Hejnová-Holubová, L. Sadílková, J. Morová, P. Sebo, RTX proteins: a highly diverse family secreted by a common mechanism, FEMS Microbiol. Rev. (2010) 1076–1112.
[6] H. Ostolaza, F.M. Goñi, Interaction of the bacterial protein toxin alpha-haemolysin with model membranes: protein binding does not always lead to lytic activity, FEBS Lett. 371 (1995) 303–306.
[7] L. Bakás, M. Veiga, A. Soloaga, H. Ostolaza, F.M. Goñi, Calcium-dependent conformation of *E. coli* alpha-haemolysin. Implications for the mechanism of membrane insertion and lysis, Biochim. Biophys. Acta 1368 (1998) 225–234.
[8] A. Soloaga, H. Ostolaza, F. Goñi, F. De la Cruz, Purification of *Escherichia coli* prohaemolysin, and a comparison with the properties of mature alpha-haemolysin, Eur. J. Biochem. 238 (1996) 418–422.
[9] S. Cavalieri, G.A. Bohach, I. Synder, *Escherichia coli* alpha-hemolysin: characteristics and probable role in pathogenicity, Microbiol. Rev. 48 (1984) 326–343.
[10] H. Ostolaza, B. Bartolomé, I. Ortiz de Zárate, F. de la Cruz, F.M. Goñi, Release of lipid vesicle contents by the bacterial protein toxin alpha-haemolysin, Biochim. Biophys. Acta 1147 (1993) 81–88.
[11] L. Bakas, H. Ostolaza, W.L.C. Vaz, F.M. Goni, Reversible adsorption and nonreversible insertion of *Escherichia coli* α-hemolysin into lipid bilayers, Biophys. J. 71 (1996) 1869–1876.
[12] V. Herlax, S. Maté, O. Rimoldi, L. Bakás, Relevance of fatty acid covalently bound to *Escherichia coli* alpha-hemolysin and membrane microdomains in the oligomerization process, J. Biol. Chem. 284 (2009) 25199–25210.
[13] R.M. Sullan, J.K. Li, C. Hao, G.C. Walker, S. Zou, Cholesterol-dependent nanomechanical stability of phase-segregated multicomponent lipid bilayers, Biophys. J. 99 (2010) 507–516.
[14] C. Dietrich, L.A. Bagatolli, Z.N. Volovyk, N.L. Thompson, M. Levi, K. Jacobson, E. Gratton, Lipid rafts reconstituted in model membranes, Biophys. J. 80 (2001) 1417–1428.

[15] L. Sánchez-Magraner, A.L. Cortajarena, F.M. Goñi, H. Ostolaza, Membrane insertion of *Escherichia coli* alpha-hemolysin is independent from membrane lysis, J. Biol. Chem. 281 (2006) 5461–5467.
[16] A. Alessandrini, P. Facci, AFM: a versatile tool in biophysics, Meas. Sci. Technol. 16 (2005) R65–R92.
[17] M.P. Mingeot-Leclercq, M. Deleu, R. Brasseur, Y.F. Dufrêne, Atomic force microscopy of supported lipid bilayers, Nat. Protoc. 3 (2008) 1654–1659.
[18] A. Alessandrini, G. Viero, M. Dalla Serra, G. Prévost, P. Facci, γ-Hemolysin oligomeric structure and effect of its formation on supported lipid bilayers: an AFM investigation, Biochim. Biophys. Acta 1828 (2013) 405–411.
[19] M. Bretscher, Membrane structure: some general principles, Science 497 (1973) 622–629.
[20] B. Engelmann, S. Streich, U.M. Schönthier, W.O. Richter, J. Duhm, Changes of membrane phospholipid composition of human erythrocytes in hyperlipidemias. I: Increased phosphatidylcholine and reduced sphingomyelin in patients with elevated levels of triacylglycerol-rich lipoprotein, Biochim. Biophys. Acta 1165 (1992) 32–37.
[21] U. Ros, M.A. Edwards, R.F. Epand, M.E. Lanio, S. Schreier, C.M. Yip, C. Alvarez, R.M. Epand, The sticholysin family of pore-forming toxins induces the mixing of lipids in membrane domains, Biochim. Biophys. Acta 1828 (2013) 2757–2762.
[22] M. Moayeri, R. Welch, Prelytic and lytic conformations of erythrocyte-associated *Escherichia coli* hemolysin, Infect. Immun. 65 (1997) 2233–2239.
[23] V.S. Herlax, M.F. Henning, A.M. Bernasconi, F.M. Goñi, L. Bakas, The lytic mechanism of *Escherichia coli* alpha hemolysin associated to outer membrane vesicles, Health 2 (2010) 484–492.
[24] G.L. Gaines, Insoluble Monolayers at Liquid–Gas Interfaces, Interscience Publishers, 1966.
[25] J. Jass, T. Tjärnhage, G. Puu, From liposomes to supported, planar bilayer structures on hydrophilic and hydrophobic surfaces: an atomic force microscopy study, Biophys. J. 79 (2000) 3153–3163.
[26] R.F. de Almeida, A. Fedorov, M. Prieto, Sphingomyelin/phosphatidylcholine/cholesterol phase diagram: boundaries and composition of lipid rafts, Biophys. J. 85 (2003) 2406–2416.
[27] M.L. Fanani, B. Maggio, Liquid–liquid domain miscibility driven by composition and domain thickness mismatch in ternary lipid monolayers, J. Phys. Chem. B 115 (2011) 41–49.
[28] K.S. Koumanov, C. Tessier, A.B. Momchilova, D. Rainteau, C. Wolf, P.J. Quinn, Comparative lipid analysis and structure of detergent-resistant membrane raft fractions isolated from human and ruminant erythrocytes, Arch. Biochem. Biophys. 434 (2005) 150–158.
[29] S. Jaikishan, J.P. Slotte, Effect of hydrophobic mismatch and interdigitation on sterol/sphingomyelin interaction in ternary bilayer membranes, Biochim. Biophys. Acta 1808 (2011) 1940–1945.
[30] J.P. Slotte, Molecular properties of various structurally defined sphingomyelins: correlation of structure with function, Prog. Lipid Res. 52 (2013) 206–219.
[31] J.P. Slotte, Sphingomyelin–cholesterol interactions in biological and model membranes, Chem. Phys. Lipids 102 (1999) 13–27.
[32] Y.J. Björkqvist, J. Brewer, L.A. Bagatolli, J.P. Slotte, B. Westerlund, Thermotropic behavior and lateral distribution of very long chain sphingolipids, Biochim. Biophys. Acta 1788 (2009) 1310–1320.
[33] X.M. Li, J.M. Smaby, M.M. Momsen, H.L. Brockman, R.E. Brown, Sphingomyelin interfacial behavior: the impact of changing acyl chain composition, Biophys. J. 78 (2000) 1921–1931.
[34] D. Marsh, Cholesterol-induced fluid membrane domains: a compendium of lipid-raft ternary phase diagrams, Biochim. Biophys. Acta 1788 (2009) 2114–2123.
[35] H.M. McConnell, A. Radhakrishnan, Condensed complexes of cholesterol and phospholipids, Biochim. Biophys. Acta 1610 (2003) 159–173.
[36] L. Bakas, A. Chanturiya, V. Herlax, J. Zimmerberg, Paradoxical lipid dependence of pores formed by the *Escherichia coli* α-hemolysin in planar phospholipid bilayer membranes, Biophys. J. 91 (2006) 3748–3755.
[37] P. Wydro, Sphingomyelin/phosphatidylcholine/cholesterol monolayers-analysis of the interactions in model membranes and Brewster angle microscopy experiments, Colloids Surf. B: Biointerfaces 93 (2012) 174–179.
[38] J.E. Shaw, R.F. Epand, J.C.Y. Hsu, G.C.H. Mo, R.M. Epand, C.M. Yip, Cationic peptide-induced remodelling of model membranes: direct visualization by in situ atomic force microscopy, J. Struct. Biol. 162 (2008) 121–138.
[39] A. Won, A. Ruscito, A. Ianoul, Imaging the membrane lytic activity of bioactive peptide latarcin 2a, Biochim. Biophys. Acta 1818 (2012) 3072–3080.
[40] M.C. Phillips, The physical state of phospholipids and cholesterol in monolayers, bilayers, and membranes, Prog. Surf. Membr. Sci. 5 (1972) 139–221.
[41] D. Marsh, Lateral pressure in membranes, Biochim. Biophys. Acta 1286 (1996) 183–223.
[42] D. Marsh, Comment on interpretation of mechanochemical properties of lipid bilayer vesicles from the equation of state or pressure–area measurement of the monolayer at the air–water or oil–water interface, Langmuir 22 (2006) 2916–2919.
[43] H.M. McConnell, Harmonic shape transitions in lipid monolayers domains, J. Phys. Chem. 94 (1990) 4728–4731.
[44] H.A. Rinia, M.M. Snel, J.P. van der Eerden, B. de Kruijff, Visualizing detergent resistant domains in model membranes with atomic force microscopy, FEBS Lett. 501 (2001) 92–96.
[45] E.I. Goksu, J.M. Vanegas, C.D. Blanchette, W.C. Lin, M.L. Longo, AFM for structure and dynamics of biomembranes, Biochim. Biophys. Acta 1788 (2009) 254–266.
[46] K.H. Sheikh, S.P. Jarvis, Crystalline hydration structure at the membrane–fluid interface of model lipid rafts indicates a highly reactive boundary region, J. Am. Chem. Soc. 133 (2011) 18296–18303.
[47] A.J. Garcia-Saez, S. Chiantia, J. Salgado, P. Schwille, Pore formation by a Bax-derived peptide: effect on the line tension of the membrane probed by AFM, Biophys. J. 93 (2007) 103–112.
[48] A.J. Garcia-Saez, S. Chiantia, P. Schwille, Effect of line tension on the lateral organization of lipid membranes, J. Biol. Chem. 282 (2007) 33537–33544.
[49] P. Schon, A.J. Garcia-Saez, P. Malovrh, K. Bacia, G. Anderluh, P. Schwille, Equinatoxin II permeabilizing activity depends on the presence of sphingomyelin and lipid phase coexistence, Biophys. J. 95 (2008) 691–698.
[50] P.O. Wu, C.R. Chiu, W.N. Huang, W.G. Wu, The role of sulfatide lipid domains in the membrane pore-forming activity of cobra cardiotoxin, Biochim. Biophys. Acta 1818 (2012) 1378–1385.
[51] G.W. Feigenson, Phase boundaries and biological membranes, Annu. Rev. Biophys. Biomol. Struct. 36 (2007) 63–77.
[52] A. Pokorny, P.F. Almeida, Permeabilization of raft-containing lipid vesicles by delta-lysin: a mechanism for cell sensitivity to cytotoxic peptides, Biochemistry 44 (2005) 9538–9544.